# Carbon dioxide generation and drawdown during active orogenesis of siliciclastic rocks in the Southern Alps, New Zealand

Catriona D. Menzies[1], Sarah L. Wright[1], Dave Craw[2], Rachael H. James[1], Jeffrey C. Alt[3], Simon C. Cox[4], Iain K. Pitcairn[5], and Damon A. H. Teagle[1]

Addresses:
[1]Ocean and Earth Science, National Oceanography Centre Southampton, University of Southampton, Southampton, SO14 3ZH, UK
[2]Department of Geology, University of Otago, Dunedin 9016, New Zealand
[3]Department of Earth and Environmental Science, The University of Michigan, 1100 North University Avenue, Ann Arbor, Michigan 48109-1005, USA
[4]GNS Science, Private Bag 1930, Dunedin 9054, New Zealand
[5] Department of Geological Sciences, Stockholm University, SE-10691 Stockholm, Sweden

Keywords
$CO_2$, mountain building, carbon isotopes, metamorphism, carbon cycle, chemical weathering

Abstract
Collisional mountain building influences the global carbon cycle through release of $CO_2$ liberated by metamorphic reactions and promoting mechanical erosion that in turn increases chemical weathering and drawdown of atmospheric $CO_2$. The Southern Alps is a carbonate-poor, siliciclastic mountain belt associated with the active Australian Pacific plate boundary. On-going, rapid tectonic uplift, metamorphism and hydrothermal activity are mobilising carbon. Here we use carbon isotope measurements of hot spring fluids and gases, metamorphic host rocks, and carbonate veins to establish a metamorphic carbon budget.
We identify three major sources for $CO_2$ within the Southern Alps: (1) the oxidation of graphite; (2) consumption of calcite by metamorphic reactions at the greenschist-amphibolite facies boundary, and (3) the dissolution of groundmass and vein-hosted calcite. There is only a minor component of mantle $CO_2$ arising on the Alpine Fault. Hot springs have molar $HCO_3^-/Ca^{2+}$ ~9, which is substantially higher than produced by the dissolution of calcite indicating that deeper metamorphic processes must dominate.

The total $CO_2$ flux to the near surface environment in the high uplift region of the Southern Alps is estimated to be ~6.4 x $10^8$ mol/yr. Approximately 87% of this $CO_2$ is sourced from coupled graphite oxidation (25%) and disseminated calcite decarbonation (62%) reactions during prograde metamorphism. Dissolution of calcite and mantle-derived $CO_2$ contribute ~10% and ~3% respectively. In carbonate-rich orogens $CO_2$ production is dominated by metamorphic decarbonation of limestones. The $CO_2$ flux to the atmosphere from degassing of hot springs in the Southern Alps is 1.9 to 3.2 x $10^8$ mol/yr, which is 30-50% of the flux to the near surface environment. By contrast, the drawdown of $CO_2$ through surficial chemical weathering ranges between 2.7 and 20 x $10^9$ mol/yr, at least an order of magnitude greater than the $CO_2$ flux to the atmosphere from this orogenic belt. Thus, siliciclastic mountain belts like the Southern Alps are net sinks for atmospheric $CO_2$, in contrast to orogens involving abundant carbonate rocks, such as the Himalaya, that are net $CO_2$ sources.

## 1. Introduction

Collisional mountain belts may have been significant sources and/ or sinks of atmospheric $CO_2$ over geological time through the generation of $CO_2$ in metamorphic reactions and drawdown of $CO_2$ during enhanced chemical weathering of silicates. Uplift of the Himalaya and Tibetan plateau and resulting enhanced weathering over the past 40 Myr has been attributed as a driving force for global late Cenozoic cooling (Raymo and Ruddiman, 1992), and orogenic cycles have undoubtedly influenced the global carbon cycle (Bickle, 1996), but the balance between $CO_2$ drawdown and release is poorly constrained and the overall effect results from variations in local climate, tectonic setting, rock type, and duration of the mountain building.

Active orogenic belts are estimated to currently be adding equivalent amounts of $CO_2$ to that from volcanoes (Kerrick et al. (1995); 0.7 to 3.5 x $10^{12}$ mol/yr of $CO_2$ from mid ocean ridges, and 1.5-3.6 x $10^{12}$ mol/yr from volcanic arcs, Kelemen and Manning (2015)). The presence of metamorphic calc-silicate minerals in high grade rocks and abundant limestones in many orogenic belts, such as the North American Cordillera, the Himalaya, the European Alps, and numerous portions of the SW Pacific Rim in Indonesia and New Guinea, is evidence that orogenic $CO_2$ is mainly generated by metamorphic decarbonation as described by the simplified Ca-endmember reaction: limestone + quartz = wollastonite + $CO_2$. In the Himalaya high grade decarbonation reactions produce abundant $CO_2$, most (~70%) of which migrates to the surface via thermal springs (0.9 x $10^{12}$ mol $CO_2$/yr for the Himalayan orogen, (Becker et al. (2008); Evans et al. (2008))).

69 Active tectonics, steep slopes, and orographic effects mean that mountain belts are
70 sites of rapid physical erosion. The resulting comminution and generation of fresh mineral
71 surfaces can lead to elevated rates of chemical weathering. Weathering of calcium silicates
72 generates a sink for $CO_2$ through reactions of the form: $2CO_2 + 3H_2O + CaAl_2Si_2O_8$
73 (anorthite) $\rightarrow Ca^{2+} + Al_2Si_2O_5(OH)_4$ (kaolinite) $+ 2HCO_3^-$ where two moles of $CO_2$ are
74 drawn down during weathering reactions although one mole is subsequently released if the
75 precipitation of marine carbonates occurs (Brady, 1991). The effectiveness of such silicate
76 weathering reactions and net drawdown of $CO_2$ remain debated, but the best estimate of
77 $CO_2$ removal rate for the present day is ~11.7 x $10^{12}$ mol $CO_2$/yr by silicate weathering and
78 ~24 x $10^{12}$ mol $CO_2$/yr total including carbonate weathering (Gaillardet et al., 1999).
79 Approximately 0.27 x $10^{12}$ mol $CO_2$/yr is drawn down through weathering reactions in the
80 Himalayan Ganges-Brahmaputra basin (Galy and France-Lanord, 1999), a factor of three to
81 four lower than the estimated release from metamorphic reactions in this region (Becker et
82 al., 2008; Evans et al., 2008).
83 In contrast, some active mountain belts, such as in Taiwan and the Southern Alps,
84 New Zealand, contain relatively few carbonate rocks and comprise siliciclastic
85 metasediments with low carbon contents (<2 wt.% C, Pitcairn et al. (2006)). These rocks
86 contain carbon as variably matured organic debris, and metamorphic interstitial carbonate
87 and veins. However, $CO_2$-effusing warm springs are also common in these mountain belts
88 (Barnes et al., 1978; Upton et al., 2011). The contribution of these low-carbon rocks to the
89 global $CO_2$ budget is poorly constrained and likely to be small. Nevertheless, the crustal
90 processes that generate this $CO_2$ in low-carbon orogenic belts are of interest, as they may
91 also be operating in the major carbonate-bearing mountain chains but are obscured by the
92 overwhelming supply of limestone-derived $CO_2$. The proportion of the total metamorphic
93 $CO_2$ flux these processes constitute will depend on the mineralogy and organic carbon
94 content of the metamorphic pile. In this paper, we evaluate the potential deep sources for
95 $CO_2$ in the active low carbon orogen of the Southern Alps, New Zealand. We define the
96 relative contributions of different key metamorphic reactions, and provide estimates of the
97 likely fluxes of $CO_2$ to the surface environment from the various deep sources within the
98 active mountain belt. This flux is then compared with estimates of $CO_2$ drawdown through
99 weathering for this area to estimate the net $CO_2$ balance for a siliciclastic orogenic belt.
100
101 1.1 Geological and tectonic setting

The South Island of New Zealand lies astride the Pacific-Australian plate boundary, and is being deformed by oblique dextral collision of these plates (Cox and Sutherland, 2007). The basement rocks are Paleozoic-Mesozoic siliciclastic metasedimentary rocks that were variably metamorphosed in the Mesozoic during terrane accretion on the margin of Gondwana (Mortimer, 2004). Since the onset of convergence along this plate boundary in the Miocene (Sutherland et al., 2000), these basement rocks are being redeformed and metamorphosed to amphibolite facies as they pass through the modern orogen in a 5 km thick zone beneath the Southern Alps (Pitcairn et al., 2014).

The metasedimentary rocks are being uplifted to form the >3000 m Southern Alps orogenic belt on the hangingwall of the Alpine Fault, the main plate boundary structure (Cox and Sutherland, 2007). Long-term, multiple-earthquake, uplift rates vary from >8 mm/yr adjacent to the Alpine Fault, to <1 mm/year in the high mountains (Main Divide region) and their eastern slopes (Outboard Zone, Fig. 1) (Norris and Cooper, 2007; Teagle et al., 1998). Erosion rates in the Inboard Zone near the Alpine fault are similar to uplift rates, so that the western slopes of the mountains retain a near steady state topographic profile, and upper greenschist to amphibolite facies metasediments are being rapidly exhumed from the middle crust (Koons, 1989). This rapid exhumation results in a high geothermal gradient, with temperatures of 350 °C as shallow as 6-8 km (Koons, 1987). Consequently the brittle-ductile transition has been raised from a regional normal of 10-12 km to form a shallow base to the seismogenic zone at ~8-10 km depth (Boese et al., 2012).

The high mountains and their eastern slopes consist of low grade (greenschist facies and lower) Mesozoic metasediments that are dominated by metagreywackes (lithic sandstones) with interlayered meta-argillites and minor metabasites (Cox and Barrell, 2007; Grapes and Watanabe, 1992) that are lithologically and geochemically similar to the high grade rocks that are being exhumed along the Alpine Fault (Fig. 1).

The principal slip zone of the Alpine Fault acts as a barrier to cross fault fluid flow throughout the crust (Menzies et al., 2016; Sutherland et al., 2012) and combined with the steep topography and the high geothermal gradient results in geothermal circulation in the Alpine Fault hangingwall (Menzies et al., 2016). Hot springs occur in deeply-incised valleys up to 17 km east of the Alpine Fault and deeper fluid flow causes deposition of hydrothermal veins from the near-surface to the middle crust (Fig. 1) (Menzies et al., 2014). The hot spring fluids commonly effervesce $CO_2$, and trapped metamorphic fluids studied in fluid inclusions in quartz veins contain abundant $CO_2$ (up to 5 mol% end member fluid, Craw and Norris (1993)).

## 2. Methods

To investigate the behaviour of carbon in the Southern Alps orogenic belt, we have analysed basement rock samples spanning an exhumed crustal cross section from prehnite-pumpellyite facies to garnet-oligoclase amphibolite facies for total carbon content, total organic carbon and carbonate content, $\delta^{13}C$ values of organic carbon/ graphite and $\delta^{13}C$ values of active geothermal fluids and calcite veins throughout the crust. This study has made use of a well chararacterised collection of rock samples taken from the full suite of metamorphic grades through the Mesozoic and Cenozoic orogens (Pitcairn et al., 2006). Samples were obtained from fresh outcrops in road cuts and river gorges. Samples of Cenozoic calcite-bearing veins were collected from amphibolite facies rocks in river gorges and glaciated exposures near the Alpine Fault (Menzies et al., 2014).

Spring waters were collected following Menzies et al. (2016) and river waters were sampled following the same protocols, although alkalinity titrations were carried out using 0.01 N $HNO_3$. Major cations in river water samples were analysed by a Perkin Elmer Optima 4300 DV ICP-OES at the National Oceanography Centre Southampton following Menzies et al. (2016). Precision and accuracy were assessed using internal reference solution SLRS4 and in-house reference solution Sco2/15 resulting in precision better than 7% and accuracy better than 6%.

Total carbon contents and total organic carbon contents were analyzed on bulk rock powders on an elemental analyzer (EA). Traces of carbonate C were removed by reaction with dilute (3N) HCl, followed by washing in distilled $H_2O$ (Könitzer et al., 2012). The $\delta^{13}C$ of TOC and TC were determined at the University of Michigan with a Costech EA coupled to a Thermo Scientific Delta V plus isotope ratio MS (IRMS), using IAEA 600 Caffeine ($\delta^{13}C$ = -27.77 ‰ VPDB) and IAEA-CH-6 Sucrose (-10.45 ‰) as calibration standards. Rock powders were degassed at 100°C and stored under vacuum to minimize adsorption of atmospheric $CO_2$. Replicate analyses of low-C content samples (<500 ppm) were within ± 70 ppm and ± 0.5 ‰ $\delta^{13}C$. Carbon blanks are less than 6% of reported C contents.

## 3. Results

### 3.1 Carbon in river and spring waters

River waters and shallow recharge groundwaters typically contain 123 to 899 µmoles/L dissolved $HCO_3^-$ (Table S1) and show a 2:1 relationship between dissolved $HCO_3^-$ and $Ca^{2+}$ that reflects calcite dissolution that involves atmospheric $CO_2$ as carbonic acid (Fig. 2). This trend is distinctly different from one which involves calcite dissolution via acid reactions

that is typical of deeper groundwaters and has a 1:1 molar relationship (Fig. 2). In contrast, spring waters show a strong trend towards high dissolved $HCO_3^-$, ranging up to 19000 μmoles/L at relatively low $Ca^{2+}$ concentrations (Fig. 2A, Menzies et al. (2016)). The dissolved carbon concentrations of these springs are minima because many effervesce of $CO_2$ and precipitate calcite as they upwell. The abundant rain on the west side of the mountains contains low concentrations of dissolved carbon (<20 μmoles/L $HCO_3^-$, Fig. 2; (Cox et al., 2015; Jacobson et al. (2003))).

When carbon is released during metamorphic decarbonation reactions the molar $HCO_3^-/Ca^{2+}$ ratio of the resulting metamorphic fluids would be significantly greater than 2 as $CO_2$ is released from carbonates and Ca sequestered in calcium silicates (Fig. 2). The high $HCO_3^-/Ca^{2+}$ ratios of warm springs in the Southern Alps (7-19) may indicate that decarbonation reactions are occurring even though carbonate is a minor component of the rock mass.

### 3.2 Rock organic carbon contents and isotope compositions

The total organic carbon (TOC) contents of the rocks are typically <0.3 wt% at all metamorphic grades, although our data suggest that the upper greenschist and amphibolite facies rocks have slightly lower TOC contents than lower grade rocks (Fig. 3a), but the difference is insignificant above 72% confidence levels. Organically derived graphitic carbon occurs in a wide range of textures across the spectrum of metamorphic grades formed during the Mesozoic (Beyssac et al., 2016). In the lowest grade rocks, the carbonaceous material is typically irregularly shaped 1-10 micron particles distributed through the relict sedimentary rock textures (Hu et al., 2015). FTIR spectra identify significant less-well ordered kerogen in carbonaceous material from unmetamorphosed greywacke to Greenschist Facies schist (Pitcairn et al., 2005). Carbonaceous material also occurs in rocks of higher metamorphic grade and in general most of this material is more mature with fewer short chain hydrocarbons, although carbonaceous material from some Amphibolite Facies Alpine Schist retain immature kerogen as shown by FTIR spectra (Pitcairn et al., 2005). The presence of immature hydrocarbons in carbonaceous material at greenschist and amphibolite facies may facilitate oxidation of rock mass carbon. Several studies have shown carbonaceous material from such metamorphic facies display evidence of graphite remobilisation in ductile and brittle shear structures (Henne and Craw, 2012; Hu et al., 2015; Kirilova et al., In Press; Pitcairn et al., 2005).

202 The $\delta^{13}C$ values of the graphitic material range between -29.5 and -17.2 ‰ (Table 1;
203 Fig. 4). As inferred Mesozoic metamorphic temperatures of the rocks increase, the $\delta^{13}C$
204 values of the graphitic material in the rocks also increase, from -26.1 ‰ (average, n = 6) in
205 low grade to prehnite-pumpellyite facies rocks to -20.4 ‰ (average, n = 8) in upper
206 greenschist and amphibolite facies rocks. Rayleigh distillation calculations suggest that the
207 carbonaceous material matured during the Mesozoic metamorphism by $CH_4$ production as
208 opposed to $CO_2$ loss (Fig. 4). Upper greenschist facies graphitic material entering the
209 Cenozoic Southern Alps orogen has $\delta^{13}C$ = -22.5 to -20.3 ‰ and the resulting amphibolite
210 facies schists exhumed adjacent to the Alpine Fault have graphitic material with $\delta^{13}C$ values
211 ranging between -22.0 and -18.5 ‰ (n = 4) (Fig.4).
212
213 3.3 Calcite contents and carbon isotope composition
214 Calcite is a minor constituent of the rock mass in the Southern Alps and commonly occurs
215 in veins (Jenkin et al., 1994; Menzies et al., 2014). The carbonate concentration of the rocks
216 does not vary significantly across metamorphic grades (Fig. 3b), the difference is
217 insignificant above 50% confidence levels. In the modern orogen, this calcite was
218 remobilised in the Alpine Fault hangingwall, and calcite is found as a vein mineral from the
219 brittle to ductile transition zone to the near surface in the Alpine Fault Zone and extends
220 further east into the Main Divide (Menzies et al., 2014). This calcite precipitated at a wide
221 range of temperatures and depths (<1 km to >6 km depth) (Jenkin et al., 1994; Menzies et
222 al., 2014).
223 Mesozoic metamorphic calcite has $\delta^{13}C$ values ranging between -11 and -6 ‰
224 (Templeton et al., 1998), in equilibrium with $CO_2$ having $\delta^{13}C$ values of -9.7 to -4.7 ‰ at
225 250 °C (using fractionation equation of Bottinga (1968)). In the Alpine Fault Zone the $\delta^{13}C$
226 values of $CO_2$ in equilibrium with calcite range between -10.1 and -3.8 ‰ (Fig. 5). Modern
227 day hot springs in the Southern Alps have $\delta^{13}C_{DIC}$ values ranging between -16.8 and -5.7 ‰
228 with an average of -9.1 ± 4 ‰ (Fig. 5, Menzies et al. (2016)), indicating $CO_2$ in the springs
229 and Cenozoic veins may be in part derived from the remobilisation of Mesozoic calcite (Fig.
230 5). However, high $HCO_3^-$ to $Ca^{2+}$ ratios in the springs (Fig. 2) preclude calcite dissolution
231 being the sole source for $CO_2$, unless significant calcium is removed by metamorphic
232 reactions. An alternative would be the shallow precipitation beneath the springs of
233 secondary non-carbonate calcium minerals, but this has not been observed.
234 4. Discussion

235 4.1 Metamorphic reactions producing $CO_2$ in Alpine Schist

236 The principal reactions involving Ca-bearing phases that occur in the Alpine orogenic
237 metamorphism from greenschist to amphibolite facies schist are the formation of oligoclase
238 and breakdown of epidote and replacement of titanite by ilmenite (eq. 2) (Grapes and
239 Watanabe, 1992). Either or both of the two carbon-bearing minerals, graphite and calcite,
240 may be involved in reactions at this metamorphic transition, but modal changes must be
241 small as their abundances are statistically similar in both greenschist facies rocks and
242 amphibolite facies hangingwall schists next to the Alpine Fault (Table 1; Fig. 3). Hence, we
243 restrict our calculations to <10% calcite and/ or graphite loss (see mass balance below,
244 Table 2).

245 Dissolved oxygen in metamorphic fluids near the greenschist-amphibolite facies
246 transition, in the presence of graphite, is negligible, with log $fO_2$ ~-45 (calculated using
247 Geochemist's Workbench). Consequently, oxidation of graphite requires redox reactions
248 that do not involve free oxygen. The reduction of epidote ferric iron to ferrous iron-bearing
249 ilmenite provides a potential redox partner for the oxidation of graphite. Greenschist facies
250 quartzofeldspathic schist contains ~4 wt.% epidote and minor greenschist facies metabasic
251 schist contains ~10 wt.% epidote (Grapes and Watanabe, 1992). This epidote is typically
252 Ps=20 at greenschist facies, so contains ~6 wt% $Fe^{3+}$ (Grapes and Watanabe, 1992).

253 $CO_2$ generated during such reactions at the greenschist-amphibolite facies transition
254 (at ~550 °C) would have $\delta^{13}C$ values of -14.4 to -7.8 ‰ which is similar to the range of
255 recorded $\delta^{13}C_{DIC}$ values in spring waters (-16.8 to -5.7 ‰), and to $\delta^{13}C$ values of $CO_2$ in
256 equilibrium with calcite veins (-11.7 to -3.8 ‰) (Fig. 5).

257 Metamorphic decarbonation of calcite is the other principal potential source of
258 metamorphic $CO_2$ (Table 2). Quartzofeldspathic schist is calcium-poor, typically containing
259 ~2 wt % CaO (Pitcairn, 2004). In greenschist facies rocks, Ca is present as calcite (~1-5
260 modal %), epidote (~4%) and titanite (~1-2%), with rare actinolite. Prograde metamorphism
261 to amphibolite facies in the Alpine orogen generates (~20%) oligoclase of $An_{20}$ from the
262 breakdown of epidote and titanite and replacement of albite. This reaction may also involve
263 the breakdown of calcite (Grapes and Otsuki, 1983) consuming Ca and releasing $CO_2$.
264 Minor metabasic schists have ~10 wt.% CaO and undergo similar mineralogical changes at
265 the greenschist to amphibolite facies transition, although they have a greater proportion of
266 epidote (10%) which breaks down to form hornblende (20%) and oligoclase (20%) at
267 amphibolite facies.

268

4.2 Mass balance at the greenschist to amphibolite facies transition

The greenschist to amphibolite facies metamorphic transformation may facilitate the release of $CO_2$, whilst consuming Ca, in order to satisfy the elevated $HCO_3^-$/ Ca ratios measured in modern day spring waters. This can be summarised with the following reaction that includes the major components in appropriate proportions (based on measured mineral modes) that consumes minor amounts of both calcite and graphite:

$$5.3NaAlSi_3O_8\ (Albite) + 0.3CaTiSiO_5\ (Titanite) + 0.7CaAl_{2.55}Fe_{0.45}Si_3O_{12}(OH)\ (Epidote) + 0.2CaCO_3\ (Calcite) + 0.08C\ (Graphite) = 5.83Na_{0.8}Ca_{0.2}Al_{1.2}Si_{2.8}O_8\ (Oligoclase) + 0.3FeTiO_3\ (Ilmenite) + 0.28CO_2 + 1.87SiO_2 + 0.33\ H_2O + 0.32Na_2O\ (goes\ into\ paragonite\ in\ mica) + 0.33O_2 \qquad eq.2$$

This reaction consumes no more than 10% of the calcite or graphite present and liberates 4.2 mmols (0.18 g) of $CO_2$ per 100 g of rock (Table 2).

To calculate the rock mass undergoing greenschist-amphibolite facies metamorphism we consider the geometry of the active orogen:

$$Rock\ mass/\ yr = CR\ x\ T\ x\ L\ x\ \rho_{rock} \quad eq.3$$

A convergence rate (CR) of 0.01 m/yr and a strike length of 100 km (L) for the most active part of the orogen and a 5 km thickness (T) for the region currently undergoing metamorphism and rock density ($\rho_{rock}$) of 2700 kg/m$^3$, processes 1.35 x $10^{10}$ kg/rock/yr. Equation 2 indicates that ~0.18 wt.% of $CO_2$ is released by calcite decarbonation and the oxidation of graphite during greenschist to amphibolite facies metamorphism, which is equivalent to 2.5 x $10^7$ kg/yr (5.7 x $10^8$ mol/yr) $CO_2$ for the Southern Alps orogen.

Alternatively, infiltrating meteoric waters have been suggested as a source of dissolved oxygen to oxidise graphite at relatively low temperatures (~150 °C, Jenkin et al. (1994)). However, the calculated $\delta^{13}C$ value of $CO_2$ generated would be greater than 0 ‰ which is substantially heavier than $\delta^{13}C$ values measured in warm springs or hydrothermal mineral veins. The ambient redox below the water table is sufficiently low that pyrite is stable and widespread implying that the amount of dissolved oxygen is too low (~log $fO_2$ of -45, calculated in Geochemist's Workbench) to permit graphite oxidation. Therefore we discount oxidation of graphite at shallow levels by oxygen dissolved in meteoric waters as a source of $CO_2$ in the orogen. In addition, the oxidation of carbonaceous material in the surficial weathering environment is also discounted as a $CO_2$ source since there is limited weathering of eroded carbonaceous material with no oxidation rinds on clasts due to short residence times (Nibourel et al., 2015).

302

303 *4.3 Composition of crustal fluids and total $CO_2$ flux to the near surface*

304 The greenschist to amphibolite facies metamorphism results in a whole rock loss of total
305 volatiles of ~1 wt.% (Pitcairn et al., 2006) equating to 1.35 x $10^8$ kg/yr of volatiles. When
306 combined with our mass balance calculations (Section 4.2) this yields a fluid containing
307 ~7.5 mol.% $CO_2$, similar to fluid inclusions in metamorphic quartz veins (~5 mol.%, Craw
308 and Norris (1993)). There is a minor mantle $CO_2$ flux from the hangingwall directly
309 adjacent (~1 km) to the Alpine Fault of 2 x $10^7$ mol/yr (Menzies et al., 2016) and including
310 this gives a total deep flux of 5.9 x $10^8$ mol/yr $CO_2$. However, because Southern Alps hot
311 springs have $HCO_3^-/Ca^{2+}$ ratios of ~9 this indicates that in addition to eq. 2 there must be a
312 minor (~10%) component of calcite dissolution either at depth, or at shallow levels in the
313 active geothermal system (<150 °C). Hence the total $CO_2$ flux is 6.4 x $10^8$ mol/yr, of which
314 87% is sourced from metamorphic graphite oxidation (25%) and decarbonation of calcite
315 (62%) at the greenschist to amphibolite facies transition, with ~10% from the shallow
316 congruent dissolution of calcite, and 3% mantle-derived.

317

318 *4.4 $CO_2$ flux to the atmosphere*

319 The flux calculated in sections 4.2 and 4.3 quantifies the amount of carbon released into the
320 near surface environment. To estimate the flux of $CO_2$ to the atmosphere from this reservoir,
321 it is necessary to quantify the proportion of $CO_2$ degassed from geothermal waters (Becker
322 et al., 2008; Evans et al., 2008). We use measured $\delta^{13}C$ values of both DIC and $CO_2$ from
323 two hot springs and combine these data with carbon isotopic fractionation factors from
324 Mook et al. (1974) for $HCO_3$-$CO_{2(g)}$ and Rayleigh fractionation modelling combined with a
325 Monte Carlo approach to estimate the likely proportion of $CO_2$ gas that is lost to the
326 atmosphere from upwelling and effusing hydrothermal waters. In the Monte Carlo
327 simulation the proportion of $CO_2$ degassed at each temperature step was randomly generated
328 between 0 and 10% over 1000 iterations of the model. This approach enabled exploration of
329 the range in possible degassing scenarios as the spring waters cool and upwell that result in
330 the measured $HCO_3$ concentrations, $\delta^{13}C_{CO2}$ and $\delta^{13}C_{DIC}$ values (Fig. 6). From these
331 simulations we are able to give realistic maximum and minimum proportions of dissolved
332 $CO_2$ degassed at each spring. The calculations are constrained by $\delta^{13}C_{CO2}$ values of -8.8 ‰
333 and $\delta^{13}C_{DIC}$ values of -3.6 ‰ and -4.8 ‰ for Fox Spring; and $\delta^{13}C_{CO2}$ values of -7.2 ‰ and
334 $\delta^{13}C_{DIC}$ values of -4.9 ‰ and -5.9 ‰ for Copland Spring (Menzies et al., 2016). The
335 difference in DIC values between the springs, and differences between $CO_2$ and DIC $\delta^{13}C$

values is likely due to temperature differences between the spring waters; Fox is ~30-40 °C and Copland ~60 °C at the surface, and isotopic fractionation factors are higher at lower temperatures (Becker et al., 2008). Silica geothermometry suggests these spring waters equilibrated with rock at ~120 °C (Menzies et al., 2016).

The model predicts that for Fox Spring degassing while cooling from 120 to 40 °C results in a net difference between DIC and $CO_2$ $\delta^{13}C$ values of 5.2 ‰. This corresponds to degassing of 30 to 50% of the total $CO_2$ during upwelling, with the higher values representing greater degassing at depth owing to smaller fractionation factors at higher temperatures. For Copland Spring the net difference between DIC and $CO_2$ $\delta^{13}C$ values is smaller, 2.3 ‰, which may be obtained through 20-30% degassing. Our data indicate that there is greater fractionation at Fox Spring, and it is unlikely that the differences in $\delta^{13}C$ values of DIC between the springs, and consequently their degassing history, is anything other than temperature-related. This indicates that greater degassing has occurred at Fox Spring, at lower temperatures, and that both fluids shared a similar deep fluid history with degassing between 20-30% followed by a further 10-20% degassing at lower temperatures at Fox Spring. Copland Spring has deposited a large travertine terrace during degassing of $CO_2$ at the surface indicating that further $CO_2$ loss occurs after it reaches the surface and it likely releases >20-30% of its initial total dissolved $CO_2$ to the atmosphere.

Using these estimates, between 30-50% of mantle and metamorphic $CO_2$ carried in hydrothermal fluids as dissolved $CO_2$ is liberated as $CO_2$ gas to the atmosphere, and the rest is added to the riverine $HCO_3^-$ budget. It is likely that there is further, limited degassing of such fluids as they flow to join the rivers, but given our wide range in estimated proportion of degassing we assume it is accounted for within this range. This allows us to revise our mountain belt $CO_2$ flux to the atmosphere from metamorphic and mantle sources to 1.9 to 3.2 x $10^8$ mol/yr over a 10 x 100 km area (1.9 to 3.2 x $10^5$ mol/km$^2$/yr). For comparison the flux of metamorphic $CO_2$ to the atmosphere from the Himalaya is estimated at 0.9 x $10^{12}$ mol/yr over a 2500 x 300 km area (1.2 x $10^6$ mol/km$^2$/yr) (Becker et al., 2008), an order of magnitude greater than the Southern Alps. The Southern Alps $CO_2$ flux calculated here is similar to the lower range of greenschist facies metamorphic $CO_2$ fluxes (0.5 to 7 x $10^6$ mol/km$^2$/yr) modelled from carbonation reaction textures in the predominantly siliciclastic Dalradian metasedimentary belt in the SW Scottish Highlands (Ronov, 1964).

*4.5 $CO_2$ drawdown by weathering processes*

To estimate the overall influence of Southern Alps orogenesis on the global atmospheric $CO_2$ budget we compare our estimated $CO_2$ flux to the atmosphere (Section 4.4) with the estimated short term rates of $CO_2$ drawdown during silicate and carbonate chemical weathering (Fig. 7, Table 3). Major ion concentrations of rivers draining to the west of the Main Divide have total, short term atmospheric $CO_2$ consumption rates of 7.5 to 39 x $10^5$ mol/km$^2$/yr (Table 3, S1 following Jacobson and Blum (2003)). Relatively high Ca/Ca+Mg+Na indicates that carbonate dissolution is the dominant chemical weathering reaction (4.2 to 31 x $10^5$ mol/km$^2$/yr). The carbonate that contributes to this weathering flux is likely sourced from disseminated carbonate veins that were deposited from hydrothermal fluids at depth, similar to what has been observed in the Himalaya (Blum et al., 1998). This is accompanied by silicate weathering (1.1 to 7.4 x $10^5$ mol/km$^2$/yr**)** at rates similar to or up to an order of magnitude higher than the global mean silicate weathering rate (9 x $10^4$ mol/km$^2$/yr, Table 3). In contrast, rivers draining to the east of the Main Divide have silicate chemical weathering rates of 0.5 to 1.3 x $10^5$ mol/km$^2$/yr (Jacobson and Blum, 2003), similar to global mean weathering rates. An additional carbon sink is the burial of particulate organic carbon exported from the mountain belt by rivers to the ocean which is estimated at 32.5 mol/km$^2$/yr and 10% of this is estimated to be stored in marine sediments on geological timescales (Hilton et al., 2008).

High rates of mechanical erosion in the Southern Alps due to rugged relief and orographic precipitation occur over a ~200 km region parallel to the Alpine Fault that extends 25 km east to the Main Divide (Jacobson and Blum, 2003). This is larger than the ~100 x 10 km region of modern convergence-related metamorphism in the most rapidly uplifting portion of the Alpine Fault hangingwall, that includes numerous warm springs that are effusing $CO_2$ to the atmosphere (Fig. 1). For this extended region west of the Main Divide the short term weathering drawdown is 0.3 to 2 x $10^{10}$ mol/yr of which 5.5 to 37 x $10^8$ mol/yr is due to silicate weathering. This is two to ten times higher than the orogenic flux of $CO_2$ from the mountain belt to the atmosphere (1.9 to 3.2 x $10^8$ mol/yr).

In the Himalaya $CO_2$ drawdown by chemical weathering is a factor of three lower than the estimated metamorphic output and therefore the Himalaya is a net source for atmospheric $CO_2$ (Becker et al., 2008). In contrast, in the Southern Alps $CO_2$ consumption by weathering is greater than $CO_2$ production, indicating that orogenic belts with low proportions of carbonate rocks may be $CO_2$ sinks. As a consequence, major continental collision events through geological time that involved dominantly siliciclastic rocks deposited before the widespread occurrence of marine carbonate sediments (Early

Proterozoic, Ronov (1964)) may have been net sinks for $CO_2$ and had the opposite influence to the modern Himalaya that dominates the modern carbon cycle (Bickle, 1996).

## Conclusions

1. The Southern Alps is a low carbon siliciclastic mountain belt developed along the transcurrent Australian Pacific plate boundary with modern uplift, metamorphism and hydrothermal activity that is mobilising carbon.
2. Hot spring $HCO_3^-/Ca^{2+}$ = 9 which is substantially higher than expected for the dissolution of calcite (1-2), indicating the operation of $CO_2$ producing and/or $Ca^{2+}$ consuming reactions in the subsurface.
3. There are three active principal sources of $CO_2$: oxidation of graphite and decarbonation of calcite at the greenschist-amphibolite facies boundary (T and P), and dissolution of rock mass calcite at shallower levels. There is only a minor component of mantle $CO_2$ coming up the Alpine Fault.
4. The total $CO_2$ flux to the near surface environment is 6.4 x $10^8$ mol/yr, of which 87% is sourced from graphite (25%) and decarbonation of calcite (62%) at the greenschist to amphibolite facies transition, 10% is from congruent dissolution of calcite, and 3% is mantle-derived.
5. The $CO_2$ flux to the atmosphere from degassing of hot springs is 1.9 to 3.2 x $10^8$ mol/yr, which is 30-50% of the flux to the near surface environment. The balance (3.2 - 4.5 x$10^8$ mol/yr) is either precipitated in subsurface veins, travertine terraces or flows into the river system as a minor component (<1-10%) of the dissolved $HCO_3^-$.
6. Rapid uplift and orographic precipitation in the Southern Alps enhances mechanical erosion, the comminution of rocks, and exposure of new reactive surface area leading to elevated rates of chemical weathering. The drawdown of $CO_2$ through this weathering ranges between 2.7 and 20 x $10^9$ mol/yr, which is at least an order of magnitude greater than the $CO_2$ flux to the atmosphere from the orogenic belt. In addition the rapid removal of particulate organic carbon from the mountain belt removes a further 16.3 x $10^9$ mol/yr of carbon (Hilton et al., 2008).
7. Although graphite oxidation and associated coupled decarbonation processes described above are also likely to occur in carbonate-rich orogens, decarbonation of limestone overwhelmingly dominates $CO_2$ production in these systems. Siliciclastic mountain belts such as the Southern Alps of New Zealand, are net sinks for

436 atmospheric $CO_2$, in contrast to orogens involving abundant carbonate rocks, such as
437 the Himalaya, that are net $CO_2$ sources.
438
439 Acknowledgements

440 C.D.M. was supported by NERC CASE PhD studentship award NE/G524160/1 (GNS
441 Science, NZ, CASE partner). D.A.H.T. acknowledges support from research grants
442 NE/H012842/1 and NE/J022128/1 and a Royal Society Wolfson Research Merit Award
443 (WM130051). S.C.C. was funded under GNS Science's "Impacts of Global Plate Tectonics
444 in and around New Zealand Programme" (PGST Contract CO5X0203). J.C.A. was
445 supported by NSF OCE 1334758. We also thank Matthew Cooper, Andy Milton, Darryl
446 Green and Lora Wingate for laboratory assistance. We thank Mike Bickle for editorial
447 advice and comments, and reviews from two anonymous reviewers that improved this
448 manuscript.
449
450
451
452
453
454
455
456
457
458
459
460
461
462
463
464
465
466
467
468

469

| Sample no. | GR_E | GR_N | Locality | Lith. | Met. Grade | Met. T (°C) | TOC wt. % | TC wt. % | $CaCO_3$ wt. % | $\delta^{13}C_{graphite}$ (‰) |
|---|---|---|---|---|---|---|---|---|---|---|
| C46 | 2409656 | 5766383 | Porters Pass | GW | Low P-P | 100 | 0.07 | 0.09 | 0.03 | -26.2 |
| C47 | 2409656 | 5766383 | Porters Pass | GW | Low P-P | 100 | 0.02 | 0.06 | 0.05 | -26.1 |
| C29 | 2293000 | 5457500 | Taieri | Pel | Low P-P | 100 | 0.54 | 0.55 | 0.01 | -22.1 |
| A68 | 2212000 | 5626000 | Hawea | Pel | P-P | 200 | 0.37 | 1.01 | 0.64 | -25.0 |
| A3 | 2265000 | 5582000 | Oturehua | Pel | P-P | 200 | 0.24 | 0.33 | 0.09 | -27.4 |
| B84 | 2150000 | 5570500 | Glenorchy | Pel | P-P | 200 | 0.06 | 0.15 | 0.09 | -29.5 |
| B14 | 2207500 | 5632500 | Hawea | Pel | Chlor GS | 300 | 0.23 | 0.42 | 0.19 | -22.3 |
| B92 | 2155000 | 5560500 | Glenorchy | Pel | Chlor GS | 300 | 0.20 | 0.22 | 0.07 | -24.1 |
| B52 | 2180900 | 5568700 | Remarks | Psam | Chlor GS | 400 | 0.02 | 1.07 | 1.05 | -22.5 |
| C72 | 2219700 | 5681300 | Pleasant Flat | QFS | Chlor GS | 400 | 0.01 | 0.22 | 0.20 | -25.5 |
| C68 | 2222900 | 5686500 | Haast | QFS | Biot GS | 500 | 0.70 | 0.87 | 0.17 | -21.0 |
| C35 | 2382844 | 5829246 | Rocky Point | QFS | Biot GS | 500 | 0.22 | 0.37 | 0.15 | -21.7 |
| C64 | 2218700 | 5688100 | Haast | QFS | Garn GS | 550 | 0.15 | 0.28 | 0.14 | -17.2 |
| C50 | 2281204 | 5746989 | Haast | QFS | Garn GS | 550 | 0.17 | 0.18 | 0.01 | -21.0 |
| C59 | 2208700 | 5687900 | Haast | QFS | G-O Amph | 600 | 0.12 | 0.13 | 0.01 | -21.1 |
| C56 | 2200900 | 5688800 | Haast | QFS | G-O Amph | 600 | 0.08 | 0.15 | 0.07 | -19.6 |
| C75 | 2197200 | 5690500 | Haast - AF | QFS | G-O Amph | 600 | 0.04 | 0.14 | 0.09 | -18.5 |
| C36 | 2368700 | 5820000 | Northern - AF | PM | G-O Amph | 600 | 0.15 | 0.31 | 0.16 | -22.0 |
| C70* | 2223100 | 5686300 | Haast | QFS | GS - Chlor | 450 | 0.11 | nd | nd | -22.5 |
| C84* | 2219200 | 5687000 | Haast | QFS | GS - Biot | 500 | 0.25 | nd | nd | -20.3 |
| C73* | 2216100 | 5688400 | Haast | MB | GS - Biot | 500 | 0.01 | nd | nd | -26.2 |
| C66* | 2222500 | 5686700 | Haast | QFS | GS - Biot | 500 | 0.29 | nd | nd | -22.5 |
| C76* | 2200900 | 5688800 | Haast | QFS | GS - Garn | 550 | 0.11 | nd | nd | -23.9 |
| C77* | 2200900 | 5688800 | Haast | QFS | GS - Garn | 550 | 0.11 | nd | nd | -21.6 |
| C50* | 2281204 | 5746989 | Franz Josef - AF | QFS | GS - Garn | 550 | 0.22 | nd | nd | -21.2 |
| C61* | 2215300 | 5688100 | Haast | QFS | GS - Garn | 550 | 0.18 | nd | nd | -18.9 |
| C56* | 2200900 | 5688800 | Haast | QFS | G-O Amph | 600 | 0.15 | nd | nd | -20.4 |
| C75* | 2197200 | 5690500 | Haast - AF | QFS | G-O Amph | 600 | 0.08 | nd | nd | -19.3 |

Table 1. Summary of carbon content and carbon isotope ratios of carbonaceous material in Southern Alps metasediments. CaCO3 contents were determined by difference between Total Carbon (TC) and Total Organic Carbon (TOC) and rounding errors result in discrepancies where $CaCO_3$+TOC to not exactly equal TC . GW = Greywacke, Pel = Pelite, Psam = Psammite, QFS = Quartzofeldspathic Schist, PM = Protomylonite, MB = metabasite. Low P-P = Low prehnite pumpellyite, P-P = Prehnite pumpellyite, Chlor GS = Chlorite Greenschist, Biot GS = Biotite Greenschist, Garn GS = Garnet Greenschist, G-O Amph = Garnet Oligoclase Amphibolite. nd = not determined, AF = Alpine Fault Lith. = lithology of the sample, Met. Grade = Metamorphic grade of the sample, Met T. = Estimated maxiumum metamorphic temperature the sample experienced. Samples with an * are from Hilton et al. (2008).

| Example rocks | Greenschist: | | Amphibolite: | | |
|---|---|---|---|---|---|
| | Wt.% | Moles | Wt.% | Moles | %Ca |
| Epidote, pS20 | 4.4 | 0.667 | 0 | 0 | 9.4 |
| Albite | 21.5 | 5.3 | 0 | 0 | |
| Calcite | 3.1 | 2 | 2.8 | 1.8 | 40 |
| Graphite | 0.21 | 0.017 | 0.2 | 0.016 | |
| Titanite | 0.9 | 0.3 | 0 | 0 | 20.3 |
| Quartz | 18.6 | 20 | 18.6 | 20 | |
| Muscovite | 24.7 | 2 | 24.7 | 2 | |
| Chlorite | 27.0 | 2.7 | 0.0 | 0 | |
| Oligoclase, An20 | 0.0 | 0 | 23.8 | 5.8 | |
| Ilmenite | 0.0 | 0 | 0.7 | 0.3 | |
| Biotite | 0.0 | 0 | 29.3 | 2 | |
| | 100.5 | | 100.2 | | |

| **Oligoclase formation:** | | | **Redox:** | | |
|---|---|---|---|---|---|
| Oligoclase, Ca | 0.72 | Ca, wt.% | Epidote > Ilmenite + $O_2$ | 0.3 | $Fe^{3+}$, wt.% |
| Titanite (Ti) | 0.19 | Ca, wt.% | (6% Fe) | 0.0047 | $Fe^{3+}$, mol |
| Epidote (Ep) | 0.41 | Ca, wt.% | Oxygen available | 0.0024 | O, mol |
| Total Ca from Ep, Ti | 0.60 | Ca, wt.% | | 0.001 | $CO_2$, mol |
| Ca required from $CaCO_3$ | 0.12 | Ca, wt.% | $CO_2$ liberated from graphite | 0.05 | $CO_2$, wt% |
| | 0.003 | Ca, mol | Total $CO_2$ | **0.18** | $CO_2$, g |
| $CO_2$ liberated, $CaCO_3$ | 0.13 | $CO_2$, g | | **4.2** | $CO_2$, mmol |

Table 2. Summary of changes in mineralogy at the greenschist to amphibolite facies transition and associated reactions that generate $CO_2$ based on mineral proportions outlined in eq. 2 and consuming no more than 10% of the carbon-bearing minerals. Changes in mineralogy match whole rock geochemistry data collected by Pitcairn (2004).

| | | area, $km^2$ | $CO_2$ x $10^5$, $mol/km^2/yr$ | $CO_2$ x $10^9$, mol/yr |
|---|---|---|---|---|
| Silicate Weathering, west of the Main Divide | max | 5000 | 7.4 | 3.70 |
| | min | 5000 | 1.1 | 0.55 |
| Carbonate Weathering, west of the Main Divide | max | 5000 | 31 | 16 |
| | min | 5000 | 4.2 | 2.1 |
| Biogenic POC, west of the Main Divide | | 5000 | 32.5 | 16.3 |
| Total Short-term drawdown | max | 5000 | 67.5 | **32.3** |
| | min | 5000 | 37.8 | **19** |
| Total Long-term drawdown | max | 5000 | 6.95 | **3.5** |
| | min | 5000 | 3.8 | **1.9** |
| Metamorphic $CO_2$ generation | | 1000 | 6.4 | 0.64 |
| Metamorphic $CO_2$ reaching atmosphere | max | 1000 | 3.2 | **0.32** |
| | min | 1000 | 1.9 | **0.19** |

Table 3. Summary of $CO_2$ drawdown through silicate and carbonate weathering, and export of particulate organic carbon (POC) from west of the Main Divide in the Southern Alps and total short term drawdown (silicate + carbonate + POC) and total long-term effective drawdown (half of silicate weathering+10% of POC) compared with crustal $CO_2$ generation and of that $CO_2$ which reaches the atmosphere.

Figure 1. a) Geological map of South Island, New Zealand coloured by metamorphic grade of the Haast Schist. Sample locations and numbers are marked. Dashed line indicates location of resistivity cross section in part b and pink dashed box outlines the area of modern day rapid uplift. b) Cross section of central South Island along dashed line A to B from Menzies et al. (2016). Zone of active metamorphism is shown as a "crustal root" beneath the orogen and down dip of the resistivity anomaly.Fig. 2a $HCO_3$ versus Ca molal contents in spring waters lie above the calcite dissolution trend lines indicating loss of Ca or addition of $CO_2$ from another source with only 10% attributed to dissolution of $CaCO_3$. b) Larger scale view of river water, groundwater and rainwater in relation to $CaCO_3$ dissolution trends. Hot Spring data from (Menzies et al., 2016).

Figure 3. a) Total organic carbon (TOC) content versus rock metamorphic temperature shows a general decrease in TOC as metamorphic temperature increases, but the difference is insignificant above 72% confidence levels as there is significant scatter in the data. b) Carbonate content versus metamorphic temperature, no trend observed. Coloured diamonds in each plot are data from the Alpine Fault. Low P-P: Low Prehnite-Pumpellyite Facies; P-P: Prehnite-Pumpellyite Facies; Chlorite GS: Chlorite Greenshist Facies; Biot GS: Biotite Greenschist Facies; Garn GS: Garnet Greenschist Facies; G-O Amph: Garnet-Oligoclase Amphibolite Facies.

Figure 4. Measured graphite $\delta^{13}C$ values versus estimated metamorphic temperature. Rayleigh distillation curves are plotted following Evans et al. (2002): $\delta f = \delta i + 1000(F^{\alpha-1}-1)$ *(eq. 1)* where, $\delta f$ is the final and $\delta i$ initial $\delta^{13}C$ values, $F$ is the mole fraction remaining in the reservoir following

removal of components and $\alpha$ is the fluid-rock fractionation factor ($CO_2$-graphite and graphite-$CH_4$ fractionation equation from Poulson (1996)). These curves describe the data when approximately 2% of the total carbon is lost as $CH_4$ every 50 °C. In this model initial carbonaceous material $\delta^{13}C$ values of -28 ‰ at 100 °C evolve to -20.7 ‰ at 600 °C, consistent with our measured data, although we note that our data display significant variation. Data highlighted by the box are representative of the isotopic composition of carbon that is going into the modern day orogen and exhumed at amphibolite facies adjacent to the Alpine Fault (pink symbols). Mesozoic fossil leaf data from de Ronde et al. (2001) and sedimentary organic carbon from Rollinson (1993).

Figure 5. Comparison of $\delta^{13}C$ values of different carbon reservoirs and outputs in the Southern Alps. $\delta^{13}C$ values of hot spring and $CO_2$ in equilibrium with Cenozoic calcite (Menzies et al., 2016) and Mesozoic calcite (Templeton et al., 1998), compared with $\delta^{13}C$ value of $CO_2$ in equilibrium with graphite at the greenschist-amphibolite facies (GS-AF) transition, and mantle $CO_2$ (Marty and Jambon, 1987).

Figure 6. Rayleigh distillation models of $CO_2$ degassing during cooling of geothermal waters at two hot springs in the Southern Alps. These models indicate that between 20 and 30% of $CO_2$ is degassed by 60 °C and a further 5-10% during cooling to 30 °C. Common initial $\delta^{13}C_{DIC}$ value at depth is taken from the average $\delta^{13}C_{HCO3}$ value calculated from carbonate veins in this area (Menzies et al., 2016). Dots represent proportion degassed and triangles are the final measured $\delta^{13}C_{DIC}$ of each spring.

Figure 7. Summary of the processes generating $CO_2$ in the Southern Alps orogen compared with rates of $CO_2$ drawdown through weathering reactions driven by elevated topography and associated enhanced erosion rates. Over short time scales the Southern Alps are a significant sink for $CO_2$ through weathering reactions, and even when considering long timescales where precipitation of marine carbonates may occur the mountain belt still acts as a net $CO_2$ sink.

547 Supplementary File:

548 1. River water data including (Jacobson et al. (2003)) data and calculations of chemical
549 weathering intensity – in spreadsheet

550

551

552 References

553

554 Barnes, I., Downes, C.J., Hurlston, J.R., 1978. Warm Springs, South Island New Zealand and their
555 potentials to yield Laumontite. American Journal of Science 278, 1412-1427.
556 Becker, J.A., Bickle, M.J., Galy, A., Holland, T.J.B., 2008. Himalayan metamorphic CO2 fluxes:
557 Quantitative constraints from hydrothermal springs. Earth and Planetary Science Letters 265, 616-
558 629.
559 Beyssac, O., Cox, S.C., Vry, J., Herman, F., 2016. Peak metamorphic temperature and thermal
560 history of the Southern Alps (New Zealand). Tectonophysics.
561 Bickle, M.J., 1996. Metamorphic decarbonation, silicate weathering and the long-term carbon
562 cycle. Terra Nova 8, 270-276.
563 Blum, J.D., Gazis, C.A., Jacobson, A.D., Page Chamberlain, C., 1998. Carbonate versus silicate
564 weathering in the Raikhot watershed within the High Himalayan Crystalline Series. Geology 26,
565 411-414.
566 Boese, C.M., Townend, J., Smith, E., Stern, T., 2012. Microseismicity and stress in the vicinity of the
567 Alpine Fault, central Southern Alps, New Zealand. Journal of Geophysical Research: Solid Earth 117,
568 B02302.
569 Bottinga, Y., 1968. Calculation of fractionation factors for carbon and oxygen isotopic exchange in
570 the system calcite-carbon dioxide-water. Journal of Physical Chemistry 72, 800-808.
571 Brady, P.V., 1991. The effect of silicate weathering on global temperature and atmospheric CO2.
572 Journal of Geophysical Research: Solid Earth 96, 18101-18106.
573 Cox, S.C., Barrell, D.J.A., 2007. Geology of the Aoraki area. Institute of Geological and Nuclear
574 Sciences 1:250 000 geological map 15. 1 sheet + 71p. Lower Hutt, New Zealand. GNS
575 Science.
576 Cox, S.C., Menzies, C.D., Sutherland, R., Denys, P.H., Chamberlain, C., Teagle, D.A.H., 2015. Changes
577 in hot spring temperature and hydrogeology of the Alpine Fault hanging wall, New Zealand,
578 induced by distal South Island earthquakes. Geofluids 15, 216-239.
579 Cox, S.C., Sutherland, R., 2007. Regional geological framework of South Island, New Zealand, and its
580 significance for understanding the active plate boundary, in: Okaya, D., Stern, T., Davey, F. (Eds.), A
581 Continental Plate Boundary: Tectonics at South Island, New Zealand. American Geophysical Union,
582 Washington DC, pp. 19-46.
583 Craw, D., Norris, R.J., 1993. Grain boundary migration of water and carbon dioxide during uplift of
584 garnet-zone Alpine Schist, New Zealand. Journal of Metamorphic Geology 11, 371-378.
585 de Ronde, C.E.J., Sibson, R.H., Bray, C.J., Faure, K., 2001. Fluid chemistry of veining associated with
586 an ancient microearthquake swarm, Benmore Dam, New Zealand. Geological Society of America
587 Bulletin 113, 1010-1024.
588 Evans, K.A., Bickle, M.J., Skelton, A.D.L., Hall, M., Chapman, H., 2002. Reductive deposition of
589 graphite at lithological margins in East Central Vermont: a Sr, C and O isotope study. Journal of
590 Metamorphic Geology 20, 781-798.
591 Evans, M.J., Derry, L.A., France-Lanord, C., 2008. Degassing of metamorphic carbon dioxide from
592 the Nepal Himalaya. Geochemistry, Geophysics, Geosystems 9, n/a-n/a.

593 Gaillardet, J., Dupré, B., Louvat, P., Allègre, C.J., 1999. Global silicate weathering and CO2
594 consumption rates deduced from the chemistry of large rivers. Chemical Geology 159, 3-30.
595 Galy, A., France-Lanord, C., 1999. Weathering processes in the Ganges–Brahmaputra basin and the
596 riverine alkalinity budget. Chemical Geology 159, 31-60.
597 Grapes, R., Otsuki, M., 1983. Peristerite compositions in quartzofeldspathic schists, Franz Josef-Fox
598 Glacier Area, New Zealand. Journal of Metamorphic Geology 1, 47-61.
599 Grapes, R., Watanabe, T., 1992. Metamorphism and uplift of Alpine schist in the Franz Josef–Fox
600 Glacier area of the Southern Alps, New Zealand. Journal of Metamorphic Geology 10, 171-180.
601 Henne, A., Craw, D., 2012. Synmetamorphic carbon mobility and graphite enrichment in
602 metaturbidites as a precursor to orogenic gold mineralisation, Otago Schist, New Zealand.
603 Mineralium Deposita 47, 781-797.
604 Hilton, R.G., Galy, A., Hovius, N., 2008. Riverine particulate organic carbon from an active mountain
605 belt: Importance of landslides. Global Biogeochemical Cycles 22, 12.
606 Hu, S., Evans, K., Craw, D., Rempel, K., Bourdet, J., Dick, J., Grice, K., 2015. Raman characterization
607 of carbonaceous material in the Macraes orogenic gold deposit and metasedimentary host rocks,
608 New Zealand. Ore Geology Reviews 70, 80-95.
609 Jacobson, A.D., Blum, J.D., 2003. Relationship between mechanical erosion and atmospheric CO2
610 consumption in the New Zealand Southern Alps. Geology 31, 865-868.
611 Jacobson, A.D., Blum, J.D., Chamberlain, C.P., Craw, D., Koons, P.O., 2003. Climatic and tectonic
612 controls on chemical weathering in the New Zealand Southern Alps. Geochimica et Cosmochimica
613 Acta 67, 29-46.
614 Jenkin, G.R.T., Craw, D., Fallick, A.E., 1994. Stable isotopic and fluid inclusion evidence for meteoric
615 fluid penetration into an active mountain belt: Alpine Schist, New Zealand. Journal of Metamorphic
616 Geology 12, 429-444.
617 Kelemen, P.B., Manning, C.E., 2015. Reevaluating carbon fluxes in subduction zones, what goes
618 down, mostly comes up. Proceedings of the National Academy of Sciences 112, E3997-E4006.
619 Kerrick, D.M., McKibben, M.A., Seward, T.M., Caldeira, K., 1995. Convective hydrothermal C02
620 emission from high heat flow regions. Chemical Geology 121, 285-293.
621 Kirilova, M., Toy, V.G., Timms, N., Halfpenny, A., Menzies, C.D., Craw, D., Beyssac, O., Sutherland,
622 R., Townend, J., Boulton, C.J., Carpenter, B.M., Cooper, A.F., Grieve, J., Little, T.A., Morales, L.,
623 Morgan, C., Mori, H., Schleicher, A., Williams, J., In Press. Textural changes of graphitic carbon by
624 tectonic and hydrothermal processes in an active plate boundary fault zone, Alpine Fault, New
625 Zealand. Geological Society of London Special Publication 453.
626 Könitzer, S.F., Leng, M.J., Davies, S.J., Stephenson, M.H., 2012. An assessment of geochemical
627 preparation methods prior to organic carbon concentration and carbon isotope ratio analyses of
628 fine-grained sedimentary rocks. Geochemistry, Geophysics, Geosystems 13, n/a-n/a.
629 Koons, P.O., 1987. Some thermal and mechanical consequences of rapid uplift: an example from
630 the Southern Alps, New Zealand. Earth and Planetary Science Letters 89, 307-319.
631 Koons, P.O., 1989. The topographic evolution of collisional mountain belts: A numerical look at the
632 Southern Alps, New Zealand. American Journal of Science 289, 1041-1069.
633 Marty, B., Jambon, A., 1987. C/3He in volatile fluxes from the solid Earth: implications for carbon
634 geodynamics. Earth and Planetary Science Letters 83, 16-26.
635 Menzies, C.D., Teagle, D.A.H., Craw, D., Cox, S.C., Boyce, A.J., Barrie, C.D., Roberts, S., 2014.
636 Incursion of meteoric waters into the ductile regime in an active orogen. Earth and Planetary
637 Science Letters 399, 1-13.
638 Menzies, C.D., Teagle, D.A.H., Niedermann, S., Cox, S.C., Craw, D., Zimmer, M., Cooper, M.J.,
639 Erzinger, J., 2016. The fluid budget of a continental plate boundary fault: Quantification from the
640 Alpine Fault, New Zealand. Earth and Planetary Science Letters 445, 125-135.
641 Mook, W.G., Bommerson, J.C., Staverman, W.H., 1974. Carbon isotope fractionation between
642 dissolved bicarbonate and gaseous carbon dioxide. Earth and Planetary Science Letters 22, 169-
643 176.

644 Mortimer, N., 2004. New Zealand's Geological Foundations. Gondwana Research 7, 261-272.
645 Nibourel, L., Herman, F., Cox, S.C., Beyssac, O., Lavé, J., 2015. Provenance analysis using Raman
646 spectroscopy of carbonaceous material: A case study in the Southern Alps of New Zealand. Journal
647 of Geophysical Research: Earth Surface 120, 2056-2079.
648 Norris, R.J., Cooper, A.F., 2007. The Alpine Fault, New Zealand: Surface Geology and Field Relations,
649 in: Okaya, D., Stern, T., Davey, F. (Eds.), A Continental Plate Boundary: Tectonics at South Island,
650 New Zealand. American Geophysical Union, Washington DC, pp. 157-175.
651 Pitcairn, I.K., 2004. Sources of fluids and metals in orogenic gold deposits: The Otago Schists, New
652 Zealand, Faculty of Science,

653 School of Ocean and Earth Sciences. University of Southampton, Southampton.
654 Pitcairn, I.K., Craw, D., Teagle, D.A.H., 2014. The gold conveyor belt: Large-scale gold mobility in an
655 active orogen. Ore Geology Reviews 62, 129-142.
656 Pitcairn, I.K., Roberts, A., Teagle, D.A.H., Craw, D., 2005. Detecting hydrothermal graphite
657 deposition during metamorphism and gold mineralisation. Journal of the Geological Society,
658 London 162, 429-432.
659 Pitcairn, I.K., Teagle, D.A.H., Craw, D., Olivio, G.R., Kerrich, R., Brewer, T.S., 2006. Sources of Metals
660 and Fluids in Orogenic Gold Deposits: Insights from the Otago and Alpine Schists, New Zealand.
661 Economic Geology 101, 1525-1546.
662 Poulson, S.R., 1996. Equilibrium mineral-fluid stable isotope fractionation factors in graphitic
663 metapelites. Chemical Geology 131, 207-217.
664 Raymo, M.E., Ruddiman, W.F., 1992. Tectonic forcing of late Cenozoic climate. Nature 359, 117-
665 122.
666 Rollinson, H.R., 1993. Using geochemical data : evaluation, presentation, interpretation. Longman
667 Scientific and Technical ; Copublished in the U.S. with J. Wiley and Sons, Harlow, Essex, England :
668 New York.
669 Ronov, A.B., 1964. Common tendencies in the chemical evolution of the earth's crust, ocean, and
670 atmosphere. Geochemistry International 4, 713-737.
671 Sutherland, R., Davey, F., Beavan, J., 2000. Plate Boundary deformation in South Island, New
672 Zealand, is related to inherited lithospheric structure. Earth and Planetary Science Letters 177, 141-
673 151.
674 Sutherland, R., Toy, V.G., Townend, J., Cox, S.C., Eccles, J.D., Faulkner, D.R., Prior, D.J., Norris, R.J.,
675 Mariani, E., Boulton, C., Carpenter, B.M., Menzies, C.D., Little, T.A., Hasting, M., De Pascale, G.P.,
676 Langridge, R.M., Scott, H.R., Reid-Lindroos, Z., Fleming, B., Kopf, A.J., 2012. Drilling reveals fluid
677 control on architecture and rupture of the Alpine Fault, New Zealand. Geology 40, 1143 - 1146.
678 Teagle, D.A.H., Hall, C.M., Cox, S.C., Craw, D., 1998. Ar/Ar dating and uplift rate of hydrothermal
679 minerals in the Southern Alps, New Zealand. Water-Rock Interaction 9, 801-804.
680 Templeton, A.S., Chamberlain, C.P., Koons, P.O., Craw, D., 1998. Stable isotopic evidence for mixing
681 between metamorphic fluids and surface-derived waters during recent uplift of the Southern Alps,
682 New Zealand. Earth and Planetary Science Letters 154, 73-92.
683 Upton, P., Craw, D., Yu, B., Chen, Y.-G., 2011. Controls on fluid flow in transpressive orogens,
684 Taiwan and New Zealand. Geological Society, London, Special Publications 359, 249-265.

685

Figure 1_colour_lowres
Click here to download Figure: Fig 1_map_lowres.pdf

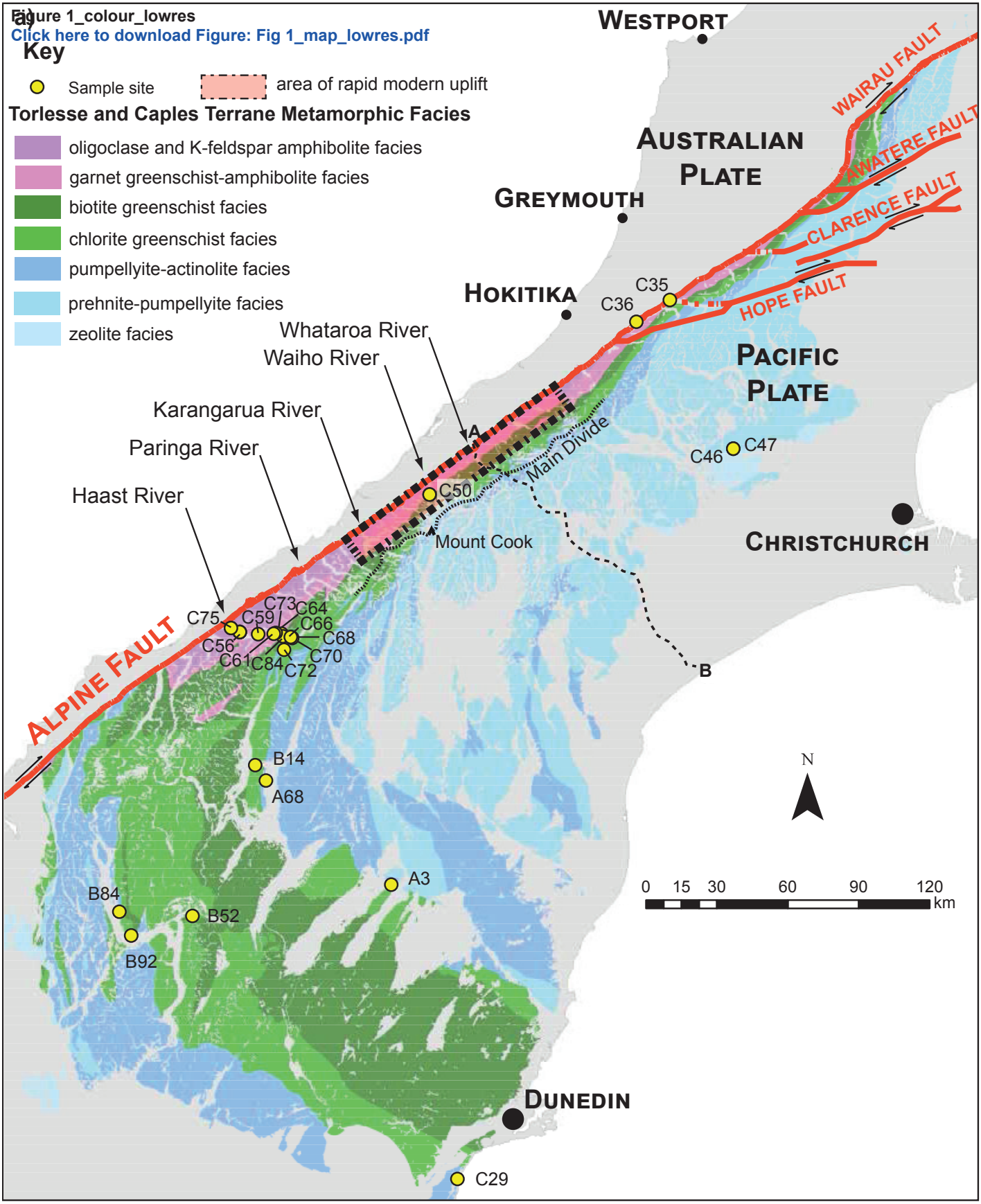


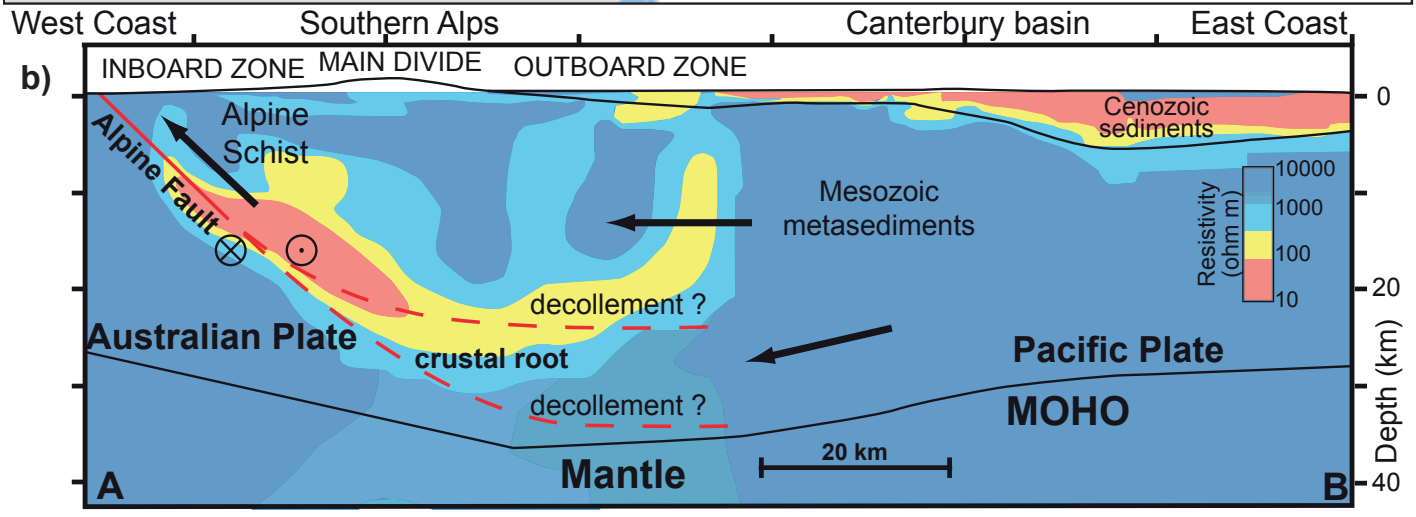

Figure 1_bw_lowres
Click here to download Figure: Fig 1_BW_lowres.pdf

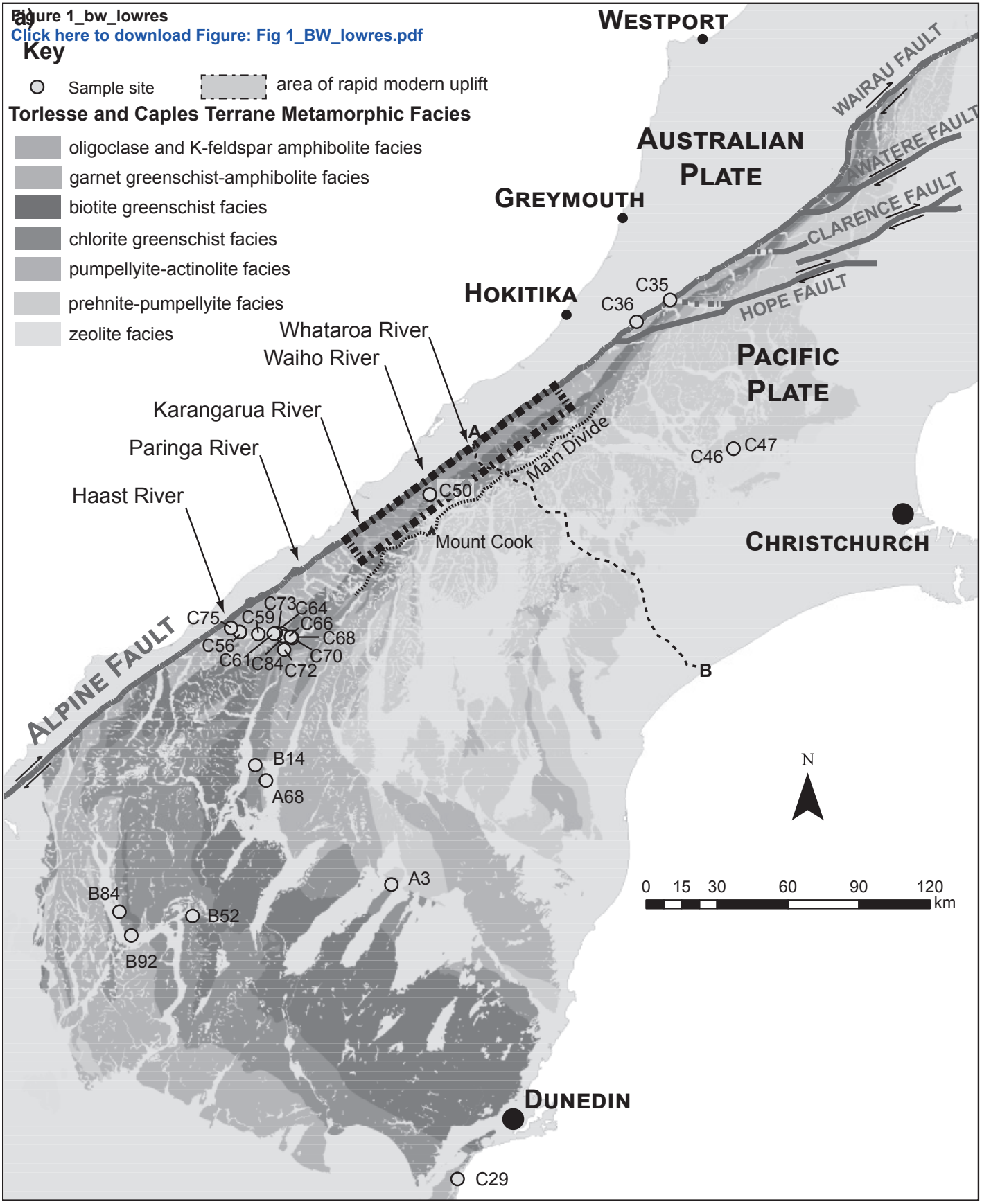


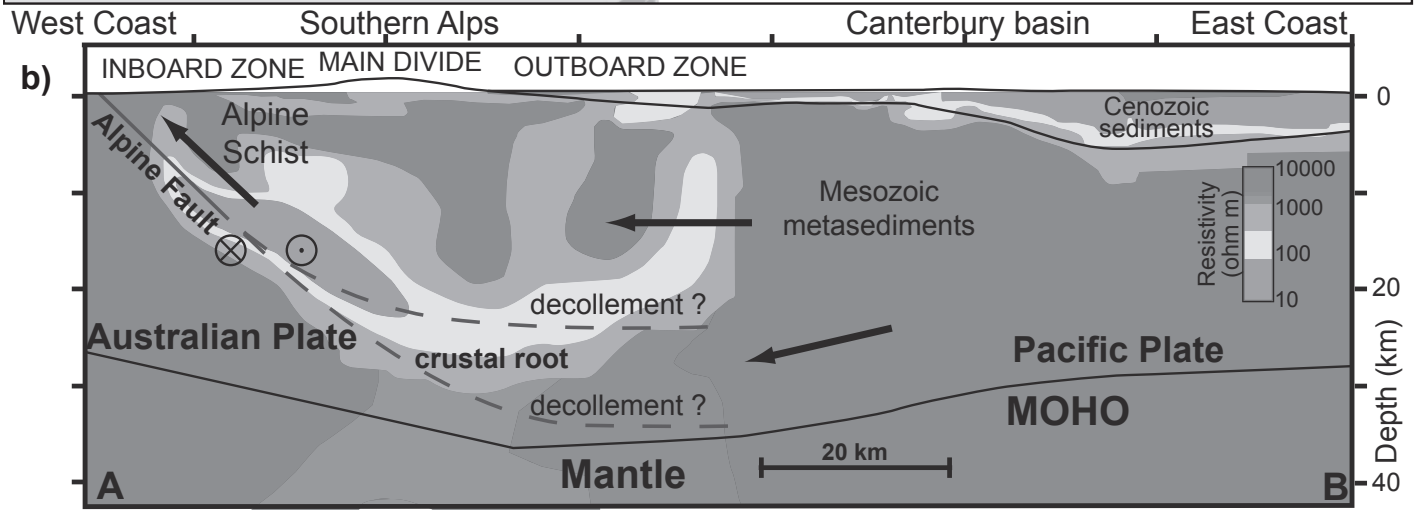

Figure 2_colour

Click here to download Figure: Fig 2_HCO3_Ca_.pdf

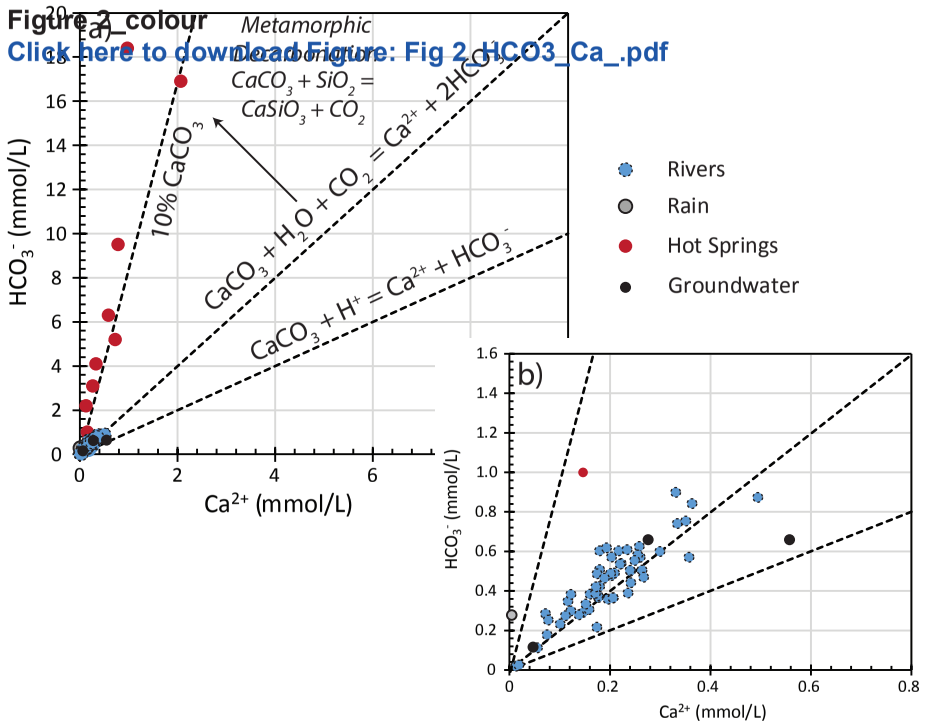

Figure 2_bw

Click here to download Figure: Fig 2_BW.pdf

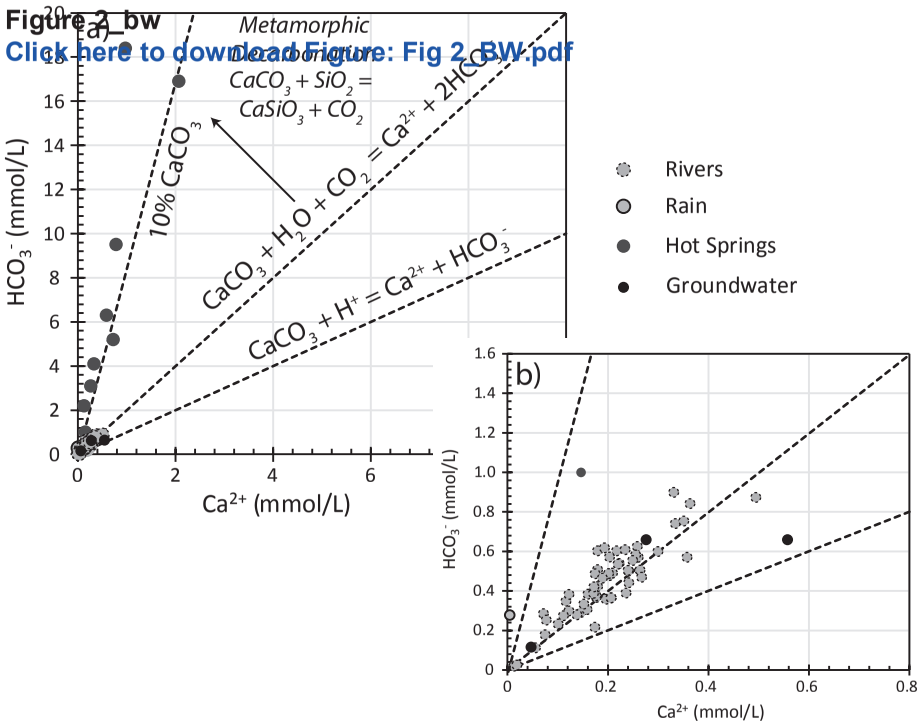

Figure 3 ~~colour~~

Click here to download Figure: Fig. 3.pdf

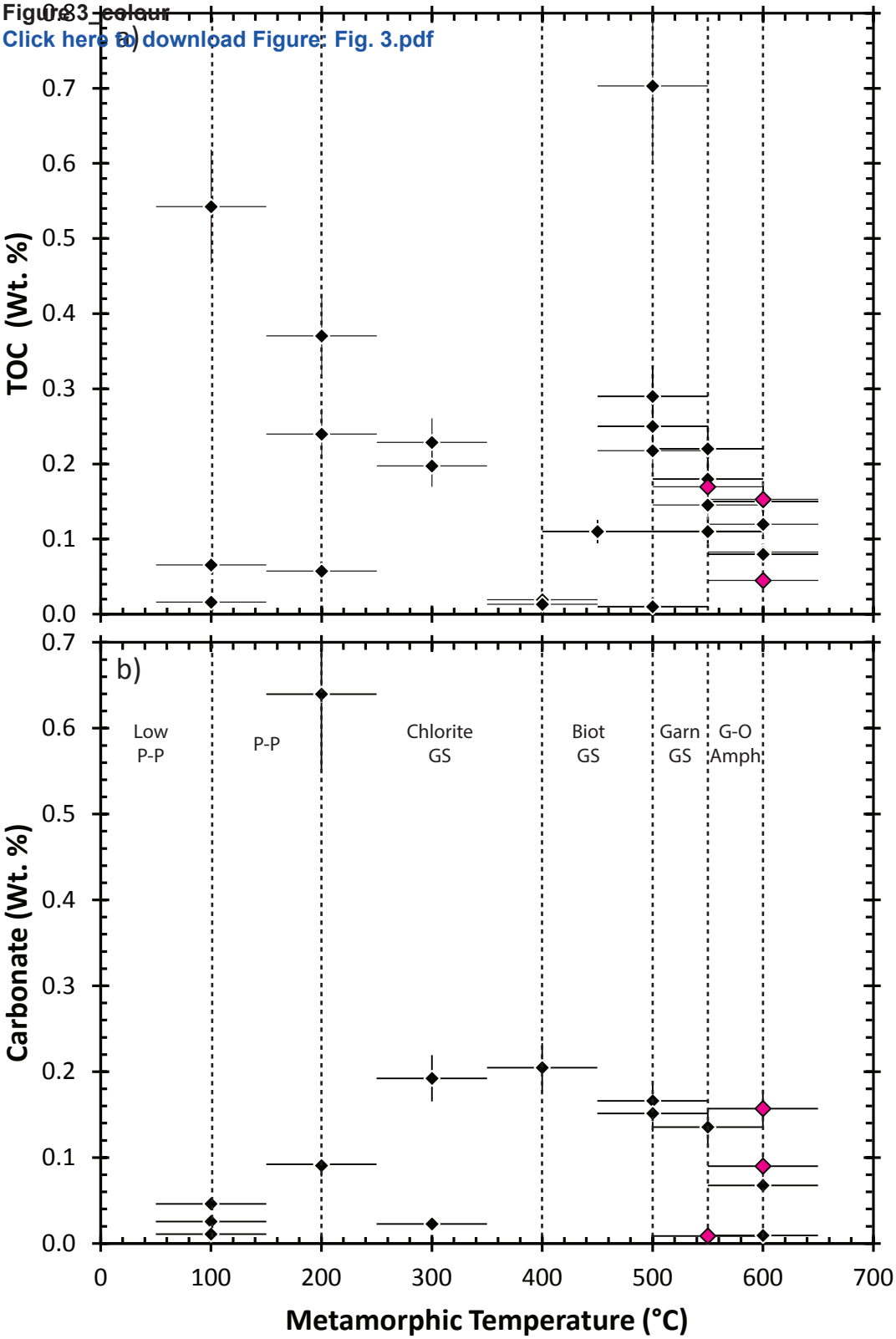

Figure 3 bw

Click here to download Figure: Fig. 3_BW.pdf

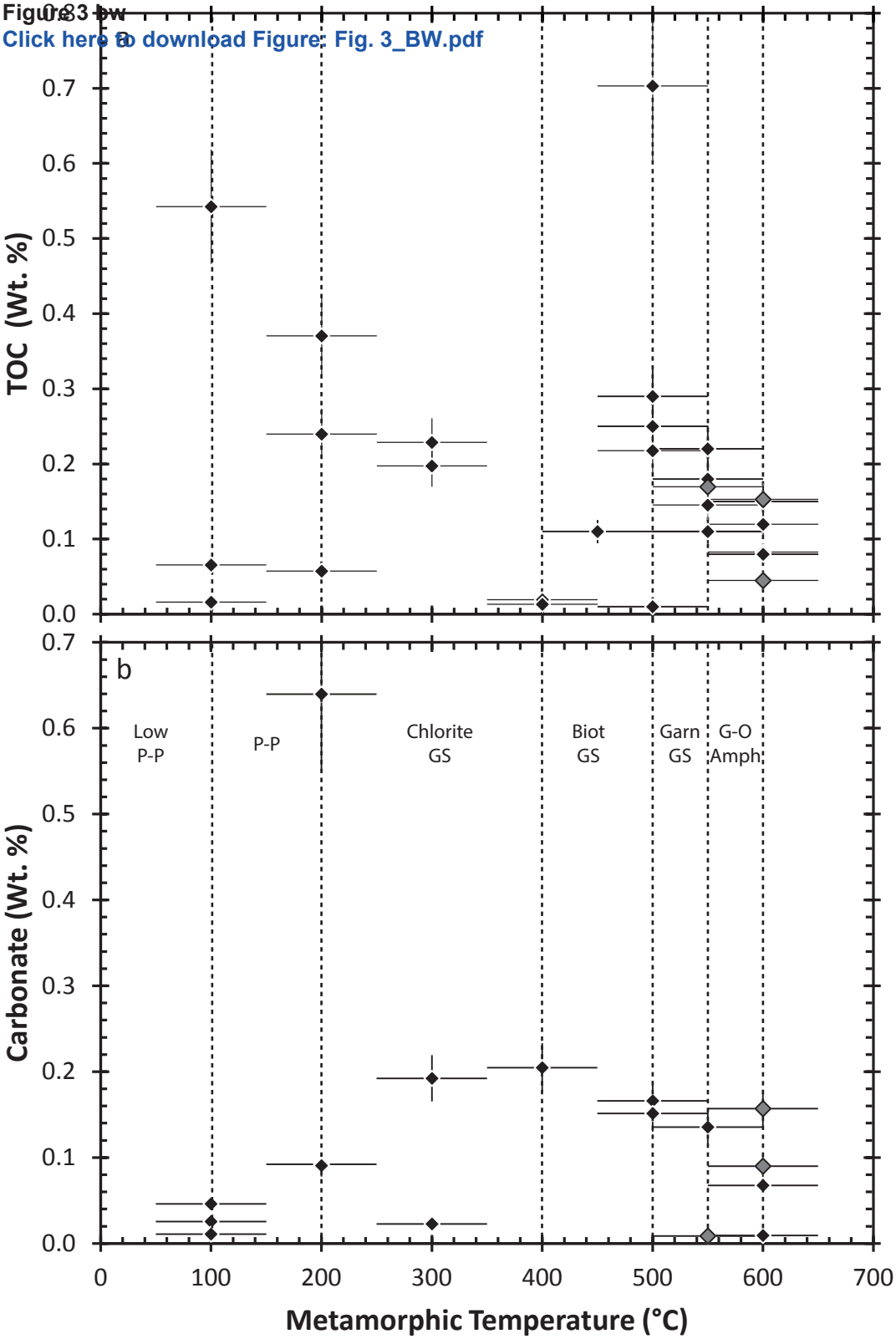

Figure 4_colour

Click here to download Figure: Fig4.pdf

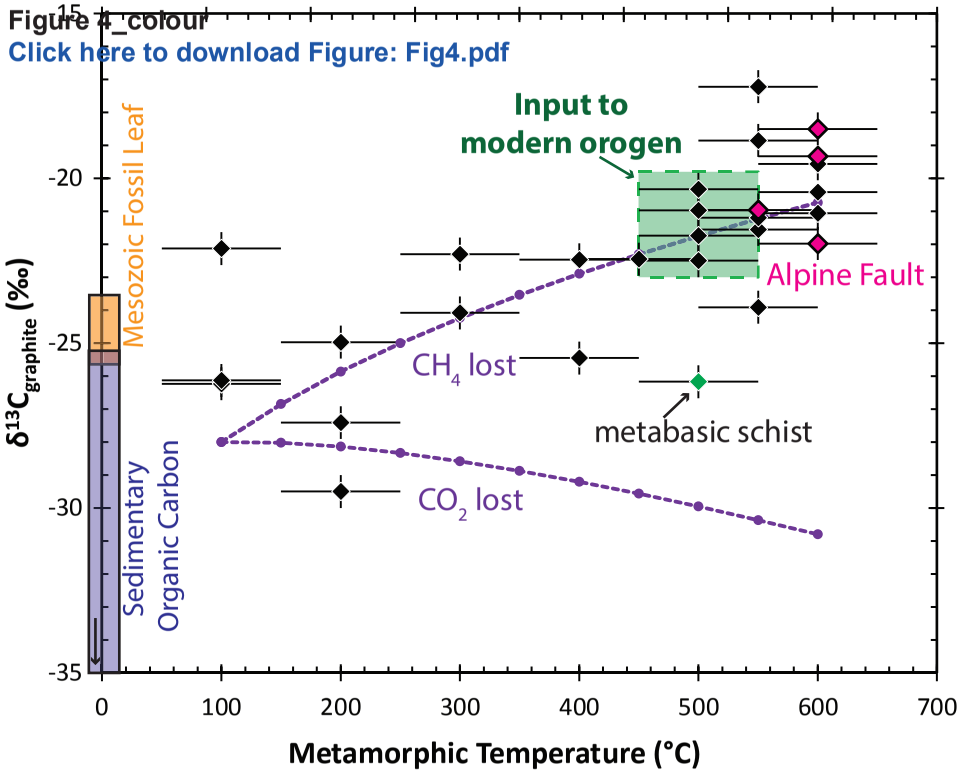

Figure 4_bw

Click here to download Figure: Fig4_BW.pdf

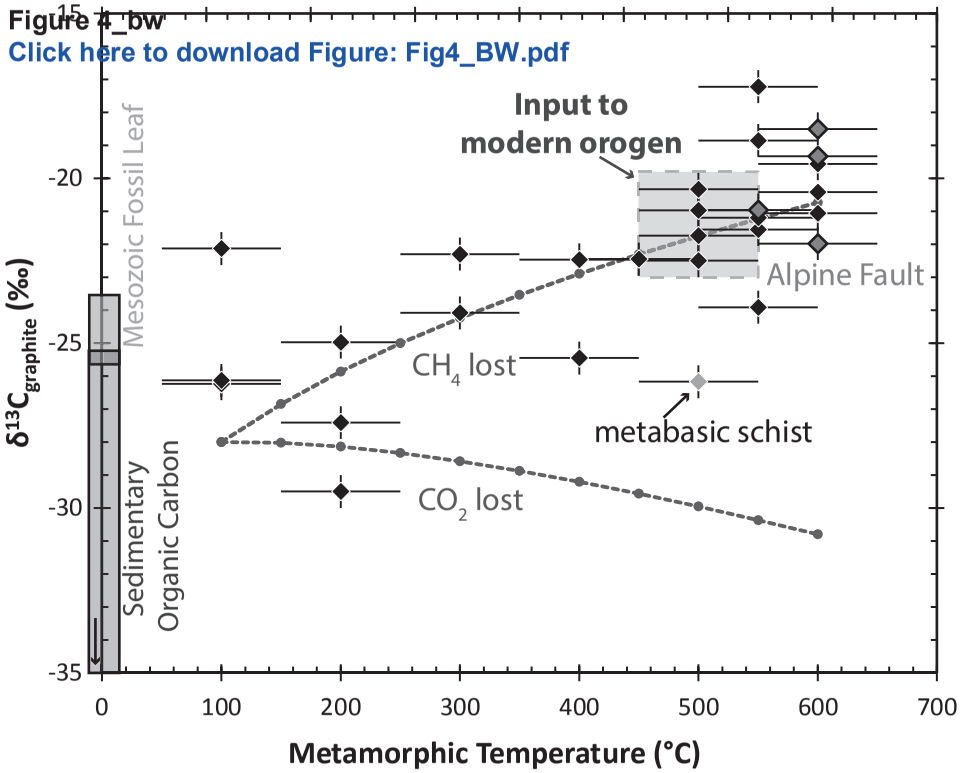

Figure 5_colour

Click here to download Figure: Figure 5.pdf

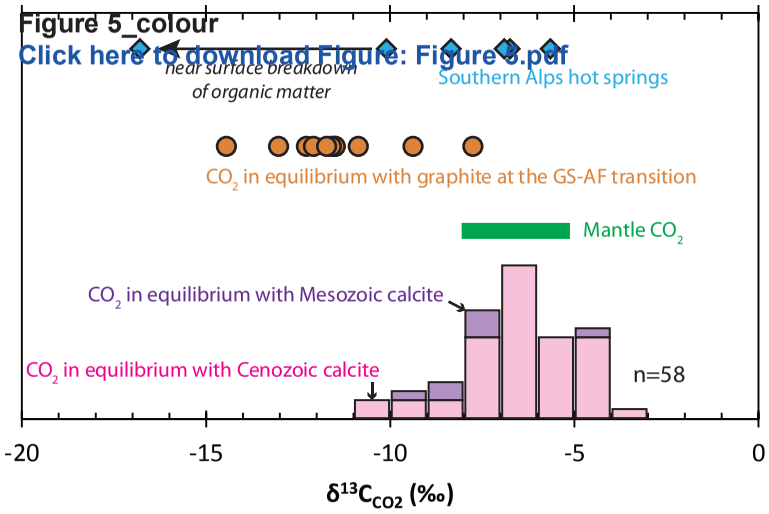

Figure 5_BW

Click here to download Figure: Figure 5_BW.pdf

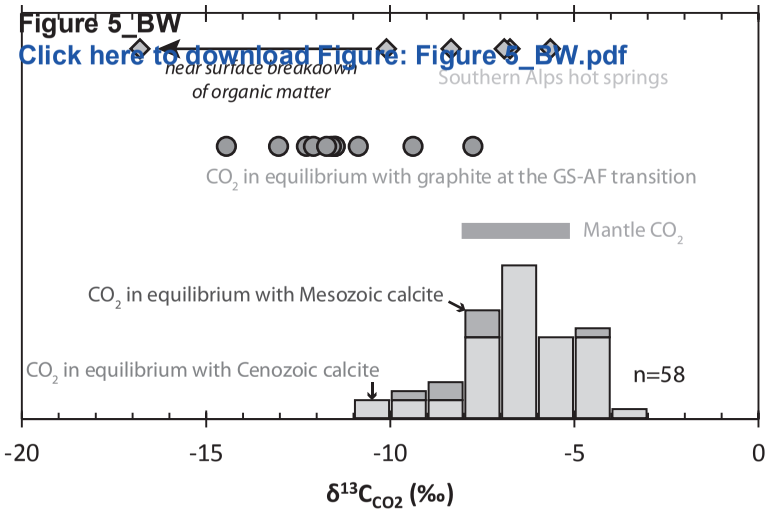

Figure 6_colour

Click here to download Figure: Figure 6.pdf

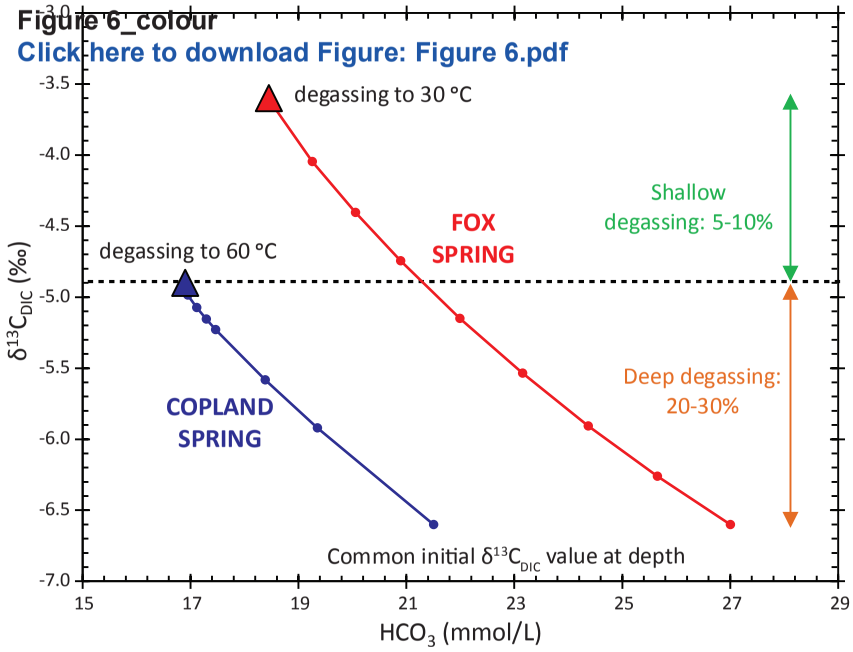

Figure 6_BW

Click here to download Figure: Figure 6_BW.pdf

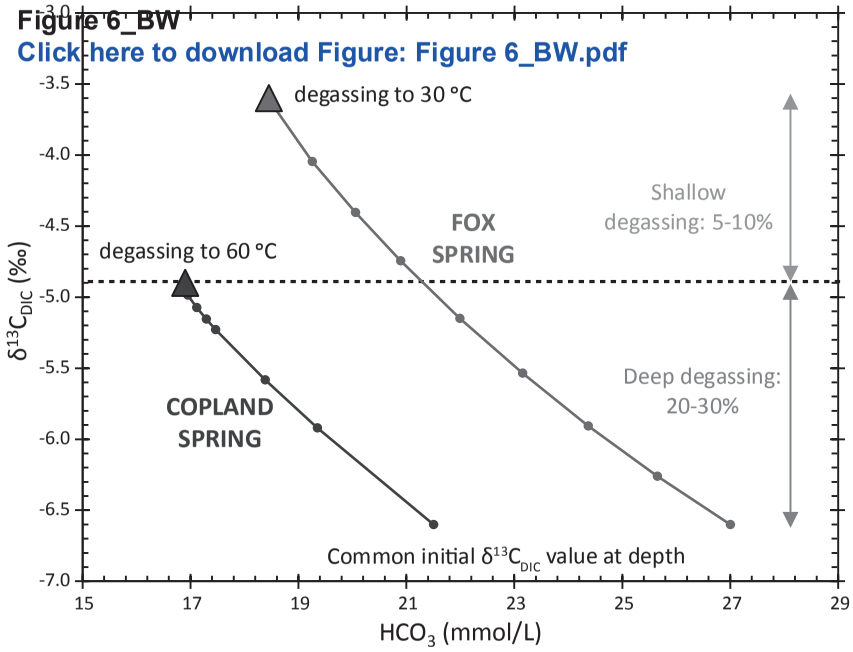

Figure 7_colour
Click here to download Figure: Figure 7.pdf

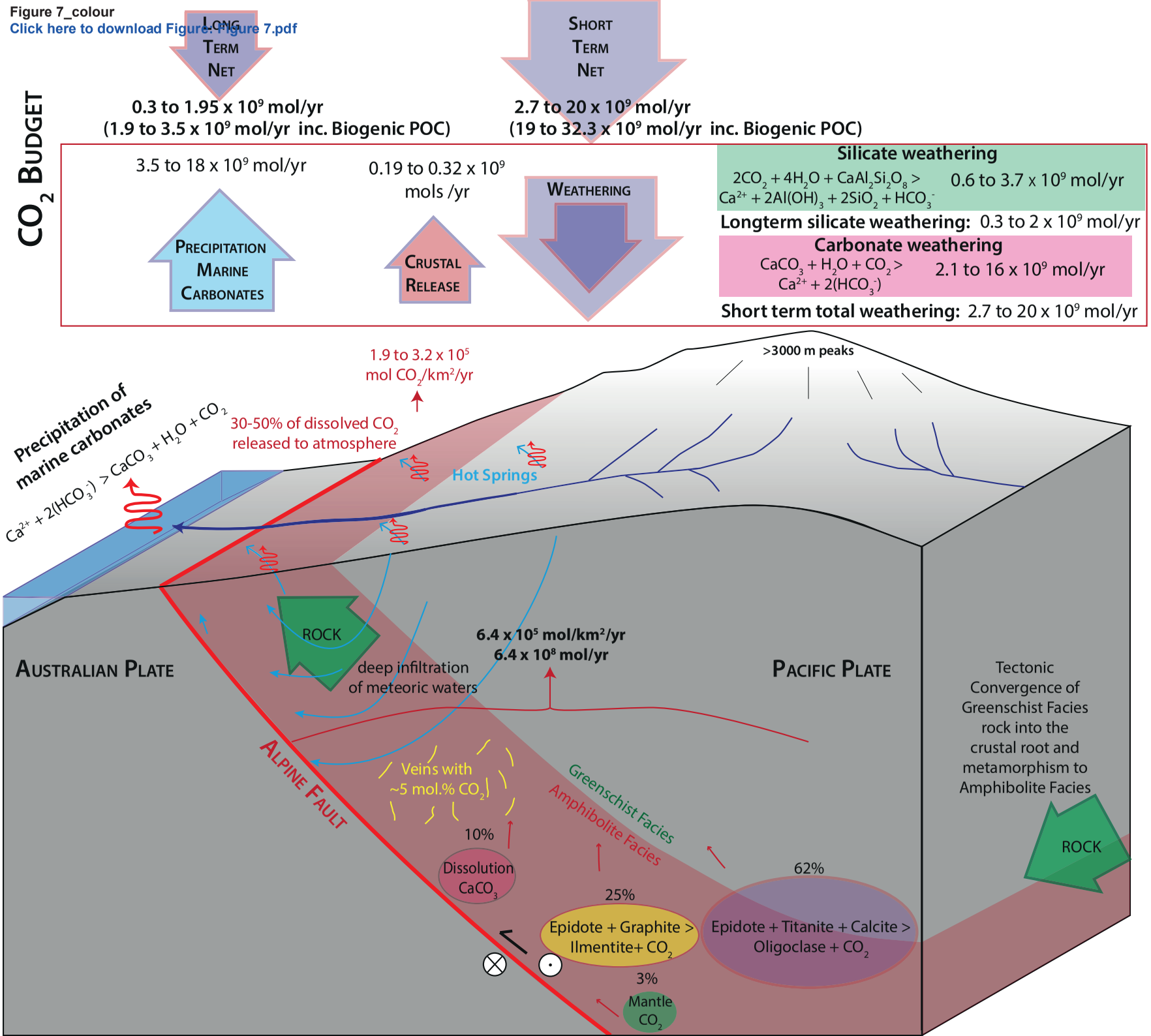

Figure 7 bw



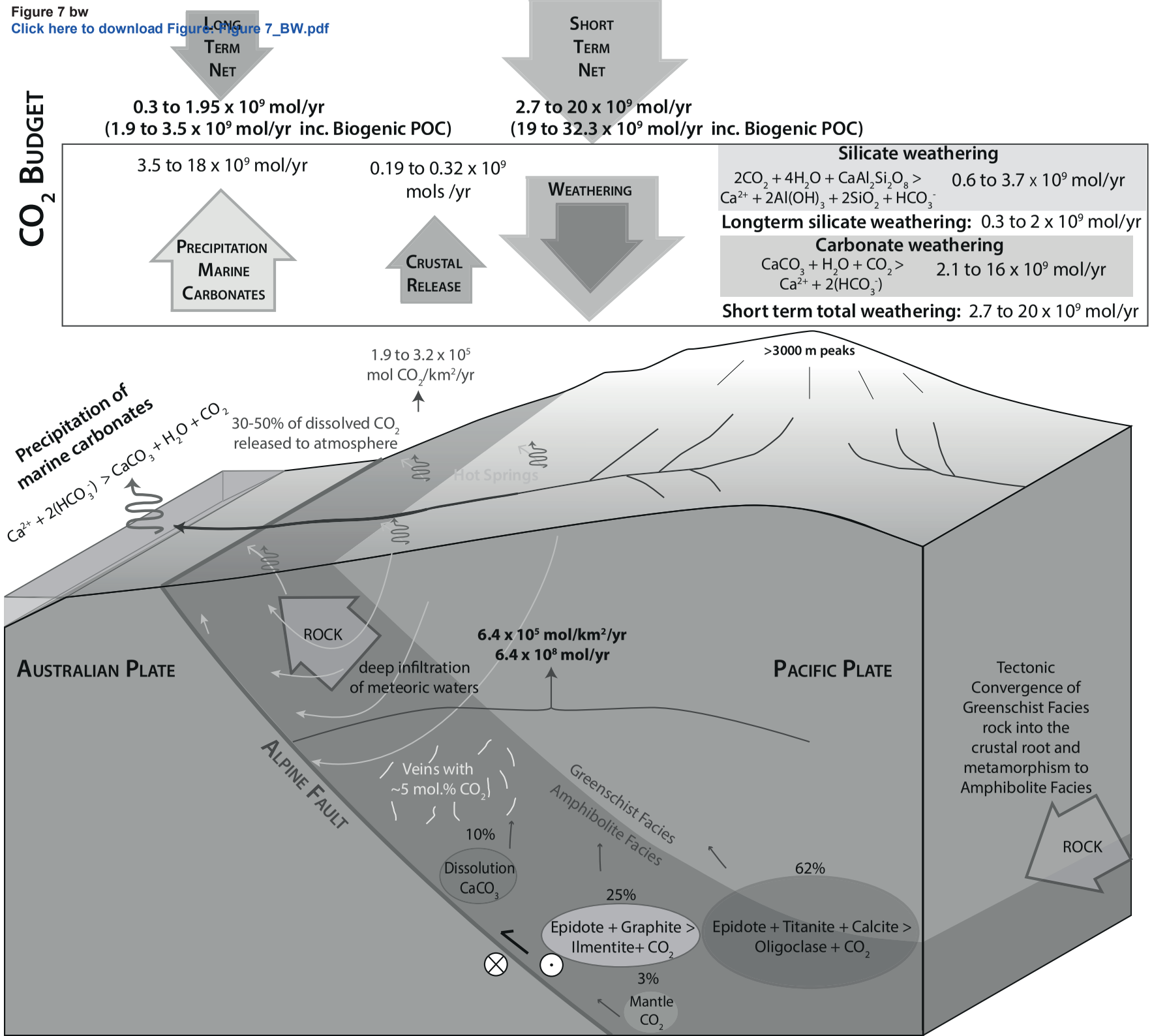

**Figure 1bw (high-resolution)**

**Click here to download Figure (high-resolution): Fig 1_BW_highres.pdf**

**Figure 1 (high-resolution)**

**Click here to download Figure (high-resolution): Fig 1_map_highres.pdf**

**Supplementary material for online publication only**

**Click here to download Supplementary material for online publication only: Supplementary File.xlsx**